



Microstructure, residual stresses and shear strength of diamond–steel-joints brazed with a Cu–Sn-based active filler alloy

Sebastian Buhl ^{a,b,*}, Christian Leinenbach ^b, Ralph Spolenak ^c, Konrad Wegener ^a

^a Institute of Machine Tools and Manufacturing, ETH Zurich, 8092 Zurich, Tannenstrasse 3, Switzerland

^b Laboratory for Joining and Interface Technology, EMPA Duebendorf, 8600 Duebendorf, Ueberlandstrasse 129, Switzerland

^c Laboratory for Nanometallurgy, ETH Zurich, 8093 Zurich, Wolfgang-Pauli-Strasse 10, Switzerland

ARTICLE INFO

Article history:

Received 23 March 2011

Accepted 16 June 2011

Keywords:

Brazing
Diamond
Residual stress
Microstructure
Shear strength

ABSTRACT

Brazing of diamonds is important in grinding technology. The brazing parameters can strongly influence the grinding tool's performance. In this work a Cu–Sn-based active filler alloy (73.9 Cu–14.4 Sn–10.2 Ti–1.5 Zr, wt.%) was applied to join monocrystalline block-shaped diamonds onto a stainless steel substrate using three different brazing temperatures (880, 930 and 980 °C) and two different dwell times (10 and 30 min), respectively. The characteristics of the joints were investigated by means of scanning electron microscopy and energy dispersive X-ray spectroscopy (microstructure and phase composition), by Raman-spectroscopy (residual stress) as well as by shear testing (bond strength). The microstructural investigations revealed an intermetallic interlayer of type Fe₂Ti at the steel–filler alloy interface, which grew with increasing brazing temperatures and longer dwell durations. The brazing parameters strongly affected the residual stresses in the diamond. Compressive residual stresses with a maximum value of –350 MPa were found in the samples brazed at 880 and 930 °C, whereas tensile stresses of maximum +150 MPa were determined in samples joined at 980 °C. The effect of the brazing parameters on the shear strength is very pronounced. The shear strength decreased from (321 ± 107) MPa at 880 °C, 10 min to (78 ± 30) MPa at 980 °C, 30 min.

© 2011 Elsevier Ltd. All rights reserved.

1. Introduction

With the increasing need to manufacture high-performance grinding tools for efficient and high-speed surface finishing of components superabrasives such as diamond and cubic boron nitride attracts more and more attention. These materials combine high hardness, high strength and high chemical inertness due to their predominant covalent lattice structure. For single-layer diamond grinding tools, active brazing is a suitable method for joining diamond grains onto a grinding tool body [1–3]. In order to attach industrial monocrystalline diamonds or chemical vapour deposition (CVD) polycrystalline diamond to metallic substrates different methods of brazing can be applied, which distinguish in the way of the heat input. The heat can be introduced e.g. by focusing a laser beam on the sample [4], by induction heating of the joining partners [5–8] or by heat radiation in a vacuum furnace [9–14]. Due to the covalent lattice structure, the presence of an active element like titanium, chromium or vanadium in the filler alloy is required for brazing of diamonds. These active elements react with diamond and change its surface in such a way that the filler alloy can wet the diamond [15]. The chemical reaction with Ti at the filler alloy–diamond interface leads to the

formation of a titanium–carbide (TiC) layer [16–18]. Cu–Sn alloys with additions of titanium belonging to the group of the high strength age hardening alloys [19,20] exhibit this required wetting behaviour [18,19,21] and form strong joints with the diamond [19]. Furthermore the Cu–Sn–Ti filler alloys exhibit a number of binary and ternary intermetallic phases [22–27] depending on the melting, cooling and annealing conditions. A good thermodynamic and crystallographic overview of the Cu–Sn–Ti system is given in [28]. The addition of small particle-sized powders, like titanium–carbide or tungsten–carbide, to the filler alloy acts as reinforcement and improves the filler alloy's abrasion resistance [12]. These particles can either be introduced mechanically into the filler alloy [12] or formed in-situ in a controlled chemical reaction between a binder and Ti during the brazing process [29].

Brazing of diamonds leads to the formation of residual stresses in the vicinity of the joining zone due to the different coefficients of thermal expansion (CTE) of the diamond, the filler alloy and the substrate. A very elegant method to quantify the residual stress in materials is the Raman-spectroscopy. It combines short measurement times with a high lateral and vertical resolution. As a result it is possible to measure stresses directly at the sites of interest, i.e. adjacent to interfaces, indents, edges, grooves and integrated circuits [30–34]. Residual stresses in the specimen are indicated by a shift of the wavenumber of the Raman–Stokes-peak compared to the wavenumber of the Raman–Stokes-peak of a stress-free specimen.

* Corresponding author. Tel.: +41 44 632 78 81; fax: +41 44 632 11 25.
E-mail address: buhl@iwf.mavt.ethz.ch (S. Buhl).

Assuming a certain stress state (uniaxial, biaxial, hydrostatic) the peak-shift can be converted into the local residual stresses.

The bond strength between the diamond and the substrate is important for grinding applications. However, only limited data can be found in the literature. Different test methods have been proposed to measure the bond strength of diamond [35–40]. Among these methods, the shear test is a meaningful experiment to characterise the effect of the brazing conditions on the joint strength. Yamazaki et al. measured the shear strength of a diamond–steel-joint brazed with a silver–copper–titanium filler alloy [39]. The shear strength values were in the range between 21 MPa and 240 MPa and depended on the cooling rate as well as on the crystallographic orientation of the diamond. In [35] the shear strength of CVD diamond on a WC–Co substrate was investigated and found to be in the range of 29 MPa to 90 MPa. In most cases the diamond film was ruptured during the loading and therefore the shear strength values are underestimated. A different setup for testing the shear strength of joints, originally developed for adhesion testing of metallic and ceramic coatings, was developed by Siegmann et al. [40]. The main advantage of this device is its easy handling, i.e. testing of simple specimen geometry, quick preparation and carrying out. Furthermore the test delivers interpretable and quantitative results of fracture mechanisms and shear strength.

The performance of metal–diamond joints is strongly depending on the microstructure, the residual stresses and the bond strength of the diamond–filler alloy and filler alloy–substrate interfaces. These parameters are strongly influenced by the processing parameters (brazing time and temperature) as well as by the filler alloy composition. In a previous work, we have studied the influence of the brazing parameters on the properties of diamond–metal joints brazed with an Ag–Cu based active filler alloy [41].

The main goal of the present work is to correlate the microstructure, the diamond's residual stresses and the shear strength of actively-brazed joints brazed with a Cu–Sn-based active filler alloy for an advanced understanding of the brazing parameters' effects on the properties of diamond–steel-joints.

2. Experimental

2.1. Materials and brazing process

In this work monocrystalline block-shaped diamonds were brazed using a Cu–Sn-based active filler alloy onto a steel substrate. The complete specimen design is shown in Fig. 1. This design was chosen since it allowed performing the microstructural investigations, the residual stress measurements and the mechanical tests on the same sample. The diamonds (Element Six e6, MT L101005Q™, Isle of Man, United Kingdom) had the dimensions 1.0 mm × 1.0 mm × 0.5 mm and were oriented on the (100) cubic plane. Three surfaces were polished, i.e. the upper and lower surface of the rectangular solid and additionally one of the lateral surfaces. This diamond type was employed because of its well-defined geometry in comparison to standard polygonal diamond grains, making it appropriate for the

intended investigations. The steel substrate consisted of the austenitic Cr–Ni–Mo stainless steel (X2CrNiMo 18–14–3, AISI 316L) and had the dimensions 10 mm × 5 mm × 30 mm. As filler alloy a powder of the commercially available Cu–Sn-based 73.9 Cu–14.4 Sn–10.2 Ti–1.5 Zr alloy (wt.%; Sulzer Metco, Hattersheim, Germany) with a liquidus temperature of 925 °C and a solidus temperature of 868 °C [16] was used. The average powder particle size was 12 μm with 10 vol.% of the particles being larger than 31 μm. In Table 1 the mechanical properties of the stainless steel substrate, of a Cu–Sn–Ti alloy with a similar composition like the filler alloy as well as of the diamond are summarised [19,42–47].

The steel substrates were cleaned from surface contaminations using acetone in an ultrasonic bath. Afterwards, they were degassed in a Torvac high-vacuum furnace for 45 min at 800 °C under high-vacuum of 10^{−5} to 10^{−6} mbar (Cambridge Vacuum Engineering LTD, Cambridge, United Kingdom). In the following step the filler alloy was placed on the substrate as a paste after drying at 150 °C. It had a thickness of about (149 ± 13 μm). The diamond was directly positioned with the lateral polished surface at the edge of the steel substrate on top of the filler alloy.

Three different brazing temperatures (880, 930 and 980 °C) and two different dwell durations (10 and 30 min) were chosen as brazing parameters. According to thermodynamic calculations, the filler alloy is only partially molten with a liquid fraction of 0.9 at 880 °C [16,17]. In general three samples were brazed within each batch, except from the batch brazed at 980 °C for 30 min for which six samples were produced. The joining processes were carried out in the above mentioned high-vacuum furnace utilising a custom-made brazing jig. A small weight (approximately 3 g) put pressure on the diamond during the whole brazing process. It prevented floating and rotating of the diamond and also improved the wetting of both parts by the molten filler alloy. After brazing, the specimens were cooled at a rate of 20 K/min in the high-vacuum furnace. In the final step, the specimens were carefully ground and polished for further investigations.

2.2. Characterisation methods

A thorough investigation of the filler alloy's microstructure was carried out using a Hitachi S-4800 high resolution scanning electron microscope (SEM, Hitachi-High Technologies, Tokyo, Japan). The atomic compositions of the developing phases were determined by means of energy dispersive X-ray spectroscopy (EDX, INCAPenta-FETx3, Oxford Instruments, High Wycombe, UK).

The micro-hardness of selected phases and reaction layers was measured using a Fischerscope HM2000 (Helmut Fischer GmbH, Sindelfingen, Germany). The measurement settings were a maximum load of 5 mN with loading and unloading times of 20 s.

Raman-spectroscopy was used for the determination of residual stresses inside the diamond. A WITec Confocal Raman Microscope 200 (WITec, Ulm, Germany) with a laser as light source (wavelength: 442 nm; Omnichrome Series 74, Melles Griot Laser Group, Carlsbad, CA, USA) was used. The resolutions in lateral and vertical dimension were 300 nm and 600 nm, respectively. The residual stresses were determined from the shift in the wavenumber ω of the Raman-

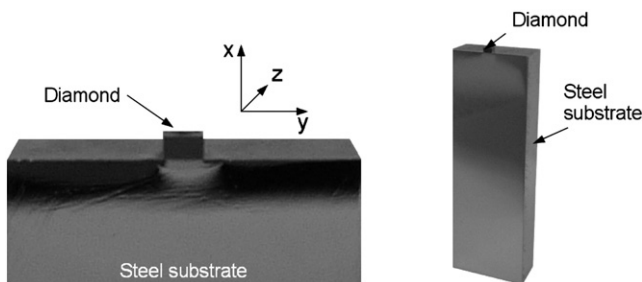


Fig. 1. Applied specimen design.

Table 1
Mechanical properties of the used materials [19,42–47].

Material	Young's modulus [GPa]	Yield strength [MPa]	Tensile strength [MPa]	CTE [10 ^{−6} /K]
X2CrNiMo 18–14–3	200	200	500–700	16.0
Cu–20Sn–10Ti	–	550	820	–
Diamond	1050	–	3750; 7500–12,500 ^a	1.1

^a Compressive fracture strength on (111) surface.

Stokes-peak of a brazed diamond compared to the wavenumber ω_0 of the Raman–Stokes-peak of an unbrazed and stress-free diamond. At room temperature the wavenumber of the diamond Raman–Stokes-peak was determined to $\omega_0 \approx 1332.2 \text{ cm}^{-1}$. All measurements were performed at room temperature under ambient condition.

Due to the geometry of the specimen (Fig. 1), which allows an unconstrained thermal expansion and contraction of the diamond in x-direction during the brazing process, an equibiaxial stress-state can be assumed. The equibiaxial residual stresses $\sigma_{\text{equibiaxial}}$ in the y–z-plane can be calculated from the shift $\Delta\omega$ in the diamond Raman–Stokes-peak according to Eq. (1):

$$\sigma_{\text{equibiaxial}} = A_{\text{equibiaxial}} \cdot (\omega - \omega_0) = A_{\text{equibiaxial}} \cdot \Delta\omega. \quad (1)$$

The proportionality factor $A_{\text{equibiaxial}}$ for diamond in this case is [48–52]:

$$\begin{aligned} A_{\text{equibiaxial}} &= 2 \cdot \omega_0 / [p \cdot (S_{11} + S_{12}) + q \cdot (S_{11} + 3 \cdot S_{12})] \\ &= -0.43 \text{ GPa} / \text{cm}^{-1} \end{aligned} \quad (2)$$

where the S_{11} and S_{12} denote the elastic compliance constants of diamond ($S_{11} = 1.01 \text{ TPa}^{-1}$, $S_{12} = -0.14 \text{ TPa}^{-1}$ [52]) and p and q are the diamond's phonon deformation potentials ($p = -2.82 \cdot \omega_0^2$, $q = -1.78 \cdot \omega_0^2$) according to [49].

Assuming that the lateral surface of the brazed diamond is stress-free, the wavenumber of the first measurement point was set as wavenumber ω_0 for the residual stress analysis as mentioned above. This resulted in stress–depth graphs, which were calculated with Eqs. (1) and (2) and averaged over 10 data points. In Fig. 2a a specimen with the various test positions for the residual stress measurements is shown. Test position No. 1 was situated approximately $10 \mu\text{m}$ above the filler alloy–diamond interface in the centre of the diamond's lateral surface. The test positions No. 2 and No. 3 were shifted $100 \mu\text{m}$ to the right and to the left and also $10 \mu\text{m}$ above the interface. The test positions No. 4 and No. 5 were at a distance of 110 and $210 \mu\text{m}$ from the filler alloy–diamond interface. The parameter “depth” indicates the measurement direction (cf. Fig. 2b) which is the direction parallel to the filler alloy–diamond interface as well as perpendicular to the polished lateral surface of the specimen. In this direction a Raman-spectrum was recorded every $0.8 \mu\text{m}$ and the wavenumber of the Raman–Stokes-peak was analysed. The analysis was performed using the programme WITec Project 1.92 (WITec, Ulm, Germany). A satisfactory Raman signal could be obtained until a maximum depth of approximately $250 \mu\text{m}$.

The shear strength of the joint was determined with a STM-20 A shear testing device (Walter + Bai AG Testing Machines, Loehningen, Switzerland). With respect to the shear testing device's design the load was introduced $50 \mu\text{m}$ above the filler alloy–diamond interface and parallel to it. A sketch is presented in Fig. 2c. Prior to testing any fillets formed during the brazing process were carefully removed using a triangular file. The tests were performed under displacement control with a shear rate of 0.1 mm/s until the joint failed. The maximum load was obtained from the load–displacement graphs and divided by the brazed diamond surface area ($A_{\text{brazed diamond}} = 1 \text{ mm}^2$) in order to obtain the shear strength. The tests were performed under ambient temperature. A more detailed description of the shear test setup is given in [40].

3. Results

3.1. Microstructural investigation

The SEM micrograph in Fig. 3 shows an overview of the whole brazing gap of a specimen brazed at $930 \text{ }^\circ\text{C}$ for 10 min. With regard to previous investigations a TiC-layer has formed at the filler alloy–diamond interface, whose thickness depends on the brazing condi-

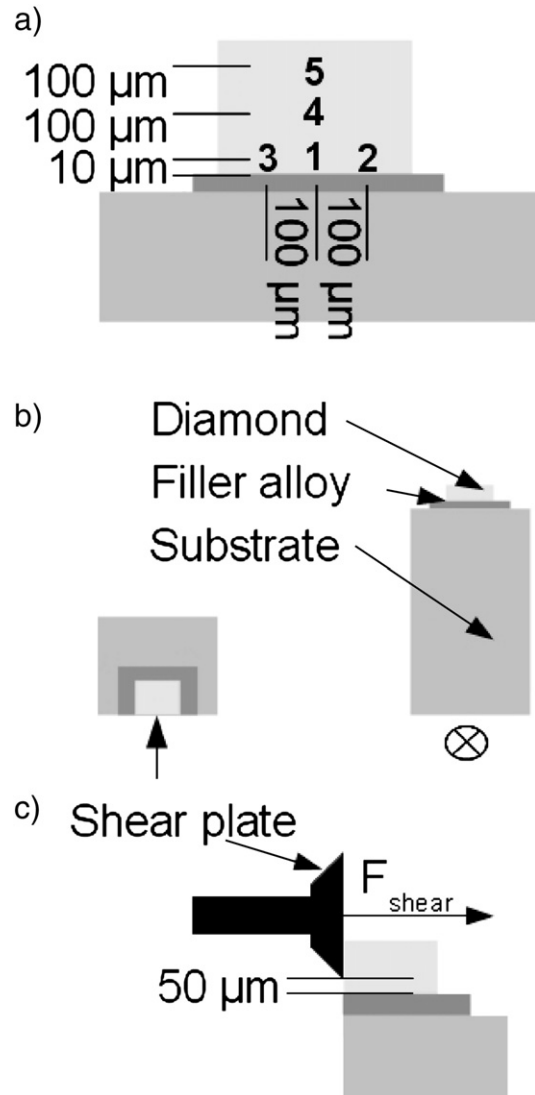


Fig. 2. Illustration of the different measurement parameters: a) test positions, b) parameter “depth”, c) schematic of the shear test.

tions [16,17]. However, this layer is difficult to identify by SEM due to its thinness ($\sim 50\text{--}250 \text{ nm}$). At the steel–filler alloy interface a titanium-containing intermetallic interlayer has developed. In-

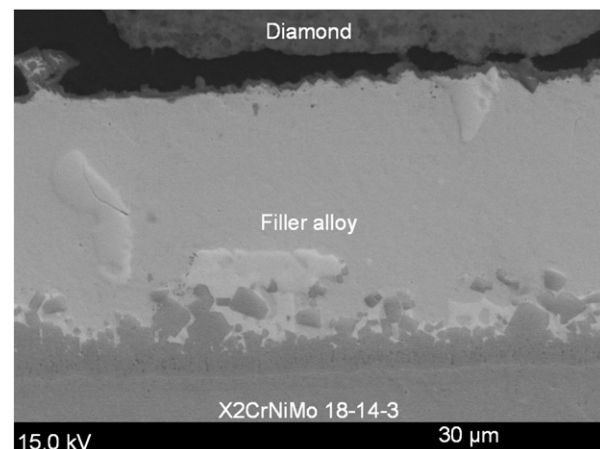


Fig. 3. Overview of the brazing gap of a joint brazed at $930 \text{ }^\circ\text{C}/30 \text{ min}$.

between these reaction interlayers the filler alloy matrix with different intermetallic phases can be seen.

In Fig. 4 the steel-filler alloy interfaces for samples brazed at 880 °C for 10 min (Fig. 4a) and at 980 °C for 10 min (Fig. 4b) are shown in detail. Directly at the steel-filler alloy interface the above mentioned intermetallic layer is clearly visible. Polygonal intermetallic crystals with the same composition are arranged ahead of this interlayer. Underneath this interlayer a diffusion zone in the steel has formed during the brazing process. In the matrix several intermetallic phases are visible differing in composition, size and morphology, as a function of the brazing conditions. The compositions of the occurring phases were measured by EDX. Based on these measurements as well as a comparison with the available phase diagram information and published literature data, the possible phases were derived, being aware that EDX measurements alone do not allow a clear identification of the phases. The intermetallic layer at the steel-filler alloy interface as well as the crystals in front of it exhibit big amounts of Fe (42.6–54.4 at.%) and Ti (26.4–36.2 at.%) as well as minor contents of Cr (9.1–15.6 at.%) and Ni (1.8–9.6 at.%) and are therefore concluded to be a $(\text{Fe,Cr,Ni})_2\text{Ti}$ -type Laves-phase [53]. The diffusion zone is characterised by a titanium amount of 7.4 at.% to 11.2 at.% in addition to the steel components. The filler matrix consists of 89.0–97.2 at.% Cu, 4.0–9.1 at.% Sn as well as traces of Ti and is therefore denoted as (Cu,Sn) -matrix (cf. Fig. 4a and b). Furthermore, three different intermetallic phases or mixtures of intermetallic phases were found. They are assumed to be CuSn_3Ti_5 (9.6–13.1 at.% Cu, 30.4–34.0 at.% Sn, 42.6–53.1 at.% Ti and 5.1–8.7 at.% Zr) as well as mixtures of CuSnTi /

Cu_2SnTi (18.0–44.2 at.% Cu, 14.3–32.9 at.% Sn, 14.8–27.9 at.% Ti and 1.8–20.0 at.% Zr) and $\text{NiSnTi}/\text{Ni}_2\text{SnTi}$ (approximately 35 at.% Ni, 24.3–24.9 at.% Sn, 15.3–15.6 at.% Ti and approximately 10 at.% Zr) [16,22–24,26,27,54–60].

Micro-hardness tests were performed on the $(\text{Fe,Cr,Ni})_2\text{Ti}$ -interlayer, on the (Cu,Sn) -matrix as well as on the $\text{CuSnTi}/\text{Cu}_2\text{SnTi}$ phase mixture. The measured micro-hardnesses, denoted in Vickers hardness or indentation hardness, were HV (169 ± 28) or (1.7 ± 0.2) GPa for the (Cu,Sn) -matrix, HV (1350 ± 70) or (14.3 ± 0.7) GPa for the $(\text{Fe,Cr,Ni})_2\text{Ti}$ -interlayer and HV (962 ± 25) or (10.3 ± 0.3) GPa for $\text{CuSnTi}/\text{Cu}_2\text{SnTi}$.

The final thickness of the brazing gap as a function of the brazing parameters is displayed in Fig. 5a. A tendency to smaller brazing gap widths with higher brazing temperatures and longer dwell durations could be observed, presuming an equal initial thickness for the different specimens. The thicknesses decreased from about 50 μm at 880 °C, 30 min to approximately 30 μm at 980 °C, 30 min. The dependence of the interlayer and diffusion zone thickness on the brazing parameters is shown in Fig. 5b. A higher brazing temperature and longer dwell duration led to a thicker diffusion zone as well as to a thicker interlayer. Comparing the thickness of the diffusion zone in the range of 880 °C to 980 °C, it highlighted that for a dwell duration of 10 min the diffusion zone's thickness doubled (from 1.1 μm to 2.2 μm), whereas it nearly tripled for 30 min holding time (from 1.7 μm to 4.9 μm). A comparison of the intermetallic interlayer thickness within the temperature range 880 °C–980 °C showed an increase of approximately 110% for 10 min dwell duration (from 3.3 μm to 7.0 μm) and of approximately 50% for 30 min (from 5.2 μm to 8.0 μm). In Fig. 5c the $(\text{Fe,Cr,Ni})_2\text{Ti}$ -crystal size as a function of the brazing parameters is shown. The crystals grew with higher brazing temperature and longer holding time from 1.4 μm (880 °C, 10 min) to 5.4 μm (980 °C, 30 min).

3.2. Residual stresses

Fig. 6a representatively shows the shift $\Delta\omega$ of the wavenumber of the diamond Raman–Stokes–peak for a brazed diamond ($\omega_0 = 1333.2 \text{ cm}^{-1}$) compared to an unbrazed one ($\omega = 1332.2 \text{ cm}^{-1}$). If the wavenumber of the Raman–Stokes–peak of a brazed diamond is higher than that of an unbrazed one, i.e. $\omega > \omega_0$, compressive residual stresses have formed in the diamond. If the Raman–Stokes–peak is shifted into the opposite direction, i.e. $\omega < \omega_0$, then tensile residual stresses are present. The accuracy of the measured wavenumber is $\pm 0.02 \text{ cm}^{-1}$, i.e. converted into residual stress, an error of about $\pm 10 \text{ MPa}$.

In Fig. 6b the stress–depth graphs determined at the five different test positions for a sample brazed at 930 °C for 10 min are shown as an example. From this figure principally three facts can be pointed out, which are also valid for other samples exhibiting compressive residual stresses. For all test positions it can be stated that the compressive residual stresses increase with increasing depth. At the test positions No. 1 to No. 3 a strong increase of the compressive residual stresses within the first 100 μm can be observed until they reach a stress plateau with almost constant residual stresses. In comparison to that, the stress–depth graphs measured at the test positions No. 4 and No. 5 show a continuous linear increase of the compressive residual stresses with increasing depth within the measuring range of 250 μm . From these measurements, however, it cannot be excluded that stress plateaus could occur at higher depths. Secondly, the stress–depth graphs close to the interface have a rather similar shape, achieving similar values of the maximum compressive residual stress in the range of -300 to -350 MPa .

A comparison of the values of the compressive residual stresses at a depth of $\sim 250 \mu\text{m}$ measured at the test positions No. 1, No. 4 and No. 5 illustrates that the compressive residual stresses decrease with increasing distance from the interface. They decrease from -350 MPa

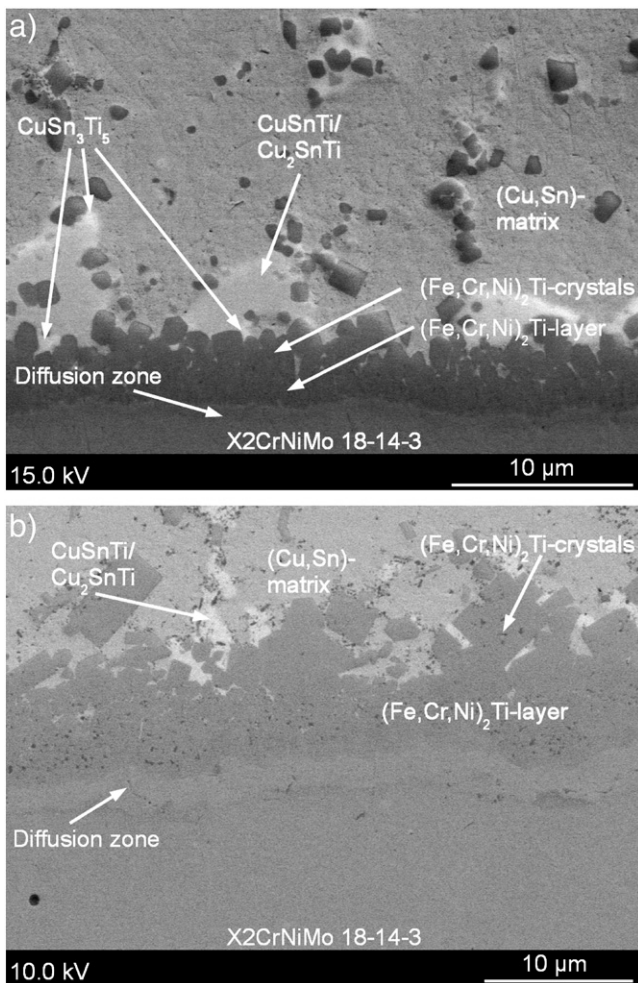


Fig. 4. Magnification of steel-filler alloy interfacial regions: a) 880 °C/10 min, b) 980 °C/10 min.

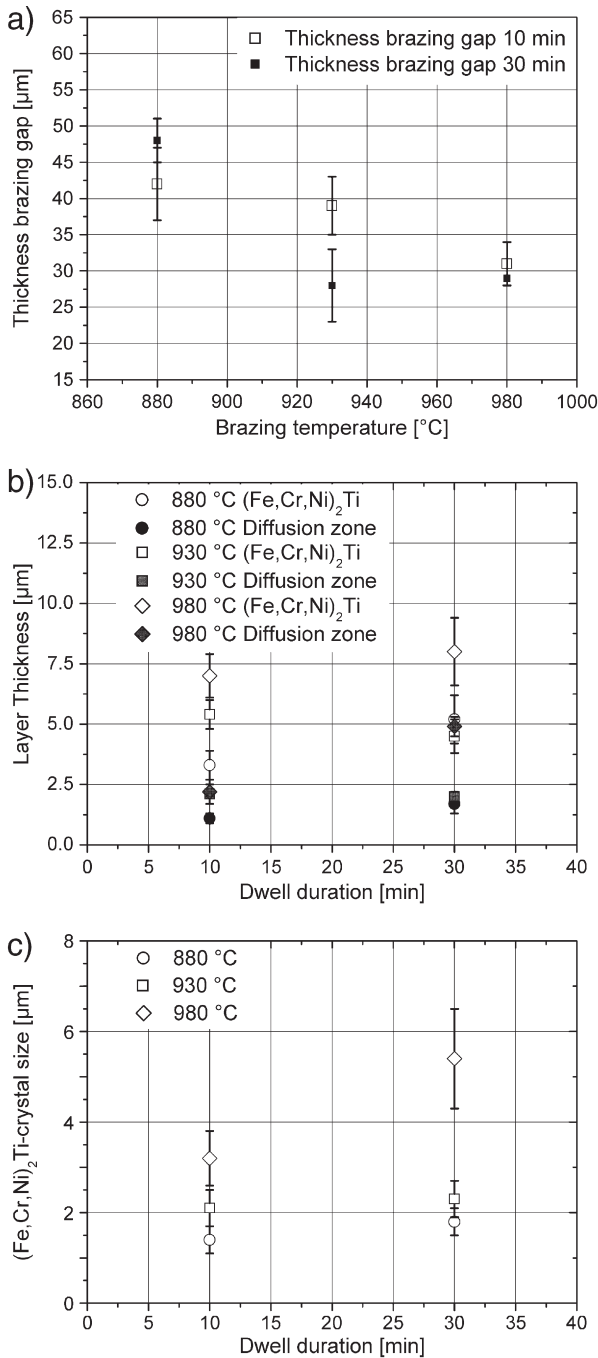


Fig. 5. Influence of the brazing parameters on the microstructural properties: a) thickness of the brazing gap, b) thickness of the interlayer and of the diffusion zone and c) crystal size.

at position No. 1 via -290 MPa at position No. 4 to -175 MPa at position No. 5. In case of the brazing parameters 980 $^{\circ}\text{C}$ for 10 and 30 min the tensile residual stress values at a depth of ~ 250 μm decrease with increasing distance to the interface.

In Fig. 7 an overview of the measured residual stresses at the test positions No. 1 (Fig. 7a), No. 4 (Fig. 7b) and No. 5 (Fig. 7c) for the different brazing parameters is given. From this figure, it becomes evident that the brazing parameters strongly influence the development of the residual stresses. The stress-depth graphs for the two lower brazing temperatures (880 and 930 $^{\circ}\text{C}$) are rather similar and indicate mainly compressive residual stresses in the diamond. However, in the vicinity of the surface to a depth of approximately 50 – 100 μm , tensile stresses in the range of 100 and 125 MPa are

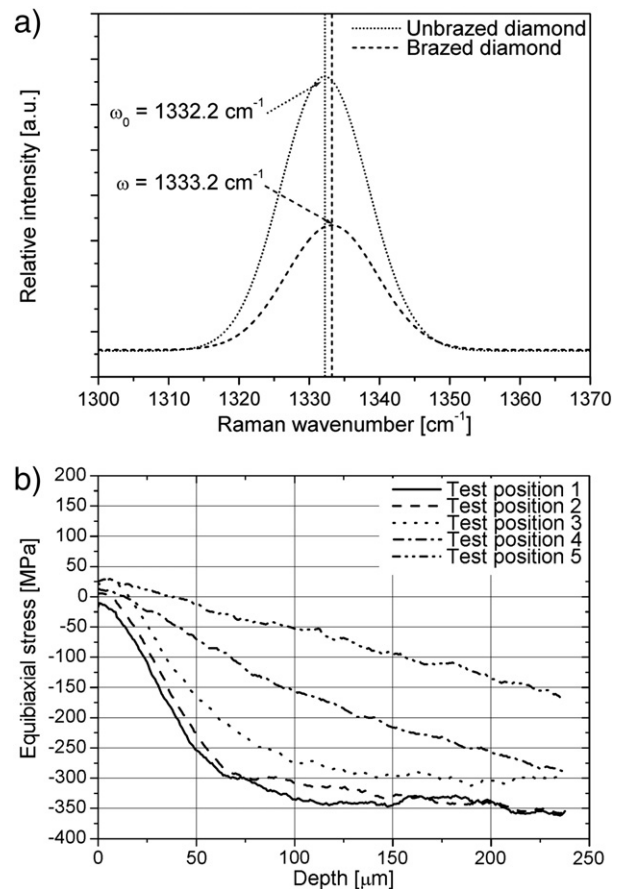


Fig. 6. Wavenumber of the Raman–Stokes peak of a braided and an unbraided diamond a) and residual stress–depth graphs for the brazing parameters 930 $^{\circ}\text{C}$ and 10 min b).

detected. Thereafter they turn into compressive stresses. At a depth of approximately 100 to 175 μm the residual stresses are reaching their stress plateaus. Furthermore the compressive residual stresses are about -75 to -100 MPa higher for 10 min holding time compared to those measured for the residual stresses determined at the test positions No. 1, No. 4 and No. 5 (cf. Fig. 7a–c). Maximum compressive residual stresses of about -350 MPa were measured in the samples brazed at 930 $^{\circ}\text{C}$ for 10 min. A higher brazing temperature of 980 $^{\circ}\text{C}$ leads to the development of tensile residual stresses in the diamond. The tensile residual stresses are $+25$ MPa and $+150$ MPa for the dwell durations of 10 and 30 min, respectively. At the test position No. 4 (Fig. 7b) the compressive residual stresses decrease by approximately -50 MPa if the brazing temperature was increased from 880 to 930 $^{\circ}\text{C}$. For the samples brazed at 980 $^{\circ}\text{C}$ the tensile residual stresses determined at test position No. 4 are lower ($\sigma_{\text{equibiaxial, max}} = +50$ MPa) compared to those measured directly at the interface. At test position No. 5 the determined compressive residual stresses are again lower for the brazing temperatures of 880 and 930 $^{\circ}\text{C}$ ($\sigma_{\text{equibiaxial}} = -100$ to -150 MPa) and the tensile residual stresses almost disappear completely (cf. Fig. 7c).

3.3. Shear strength and fracture behaviour

The mean values of the shear strength of the diamond–steel-joints as a function of the different brazing parameters and the corresponding standard deviations are shown in Fig. 8. The shear strength values are listed in Table 2. For a brazing temperature of 880 $^{\circ}\text{C}$ the mean shear strength values are (321 ± 107) MPa and (221 ± 87) MPa for 10 and 30 min holding time, respectively. The shear strength decreases with increasing brazing temperature. Specimens brazed at 930 $^{\circ}\text{C}$ for

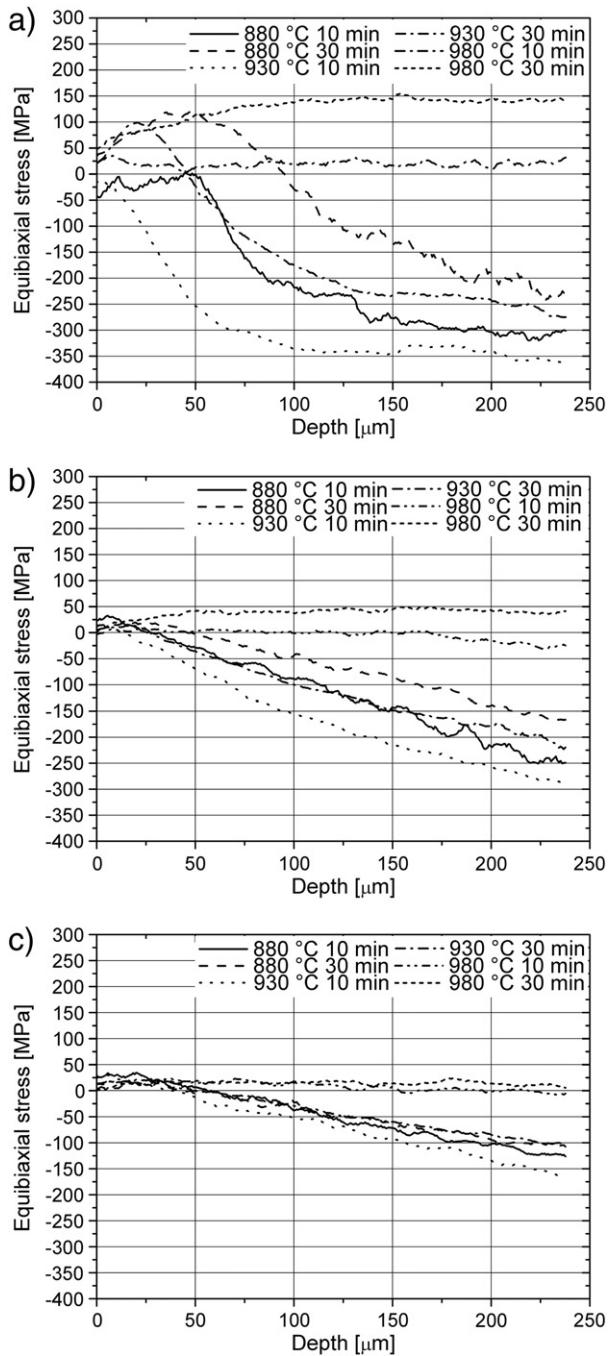


Fig. 7. Effect of the brazing parameters on the development of the residual stresses at the test positions No. 1 a), No. 4 b) and No. 5 c).

10 min had shear strength of (199 ± 18) MPa, which further decreased to (140 ± 25) MPa when brazed for 30 min. The samples brazed at 980 °C have the lowest shear strengths, independent of the two investigated dwell durations. The shear strengths are (71 ± 9) MPa for 10 min and (78 ± 30) MPa for 30 min dwell duration, respectively. In order to interpret the results of the shear tests the fracture surfaces of the failed samples were investigated by SEM.

Fig. 9a–e presents the SEM micrographs of the fracture surfaces on the steel substrate (a, c and e) as well as on the diamond side (b, d and f). The samples were brazed at 880 °C, 10 min (a and b), at 930 °C, 10 min (c and d) and at 980 °C, 10 min (e and f). In general four different fracture mechanisms are identified; they are a partially ductile shearing of the filler alloy, brittle fracture in the intermetallic

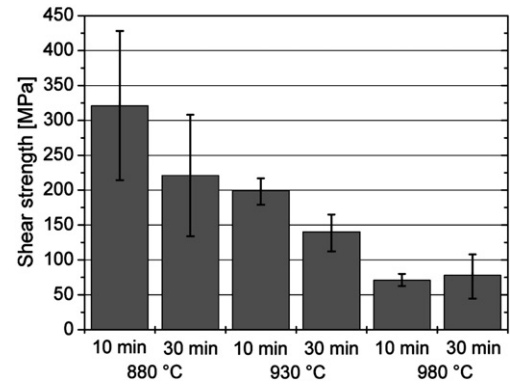


Fig. 8. The diagram shows the shear strength mean values with their corresponding standard deviations.

interlayer, failure in the TiC-layer as well as partial destruction of the diamond.

The shear surface on the steel substrate for the sample brazed at 880 °C, 10 min (sample No. 2) exhibits rough areas next to smooth ones (see Fig. 9a). The rough areas are sheared filler alloy still adhering to the diamond (cf. Fig. 9b). The smooth surfaces are identified to be parts of the TiC-layer, as could be proved by EDX measurements. In Fig. 9c the fracture surface on the steel substrate for a sample brazed at 930 °C for 10 min (sample No. 3) is shown. Here different fracture features can be seen. These are fracture in the brittle $(\text{Fe,Cr,Ni})_2\text{Ti}$ -interlayer and directly at the filler alloy-diamond interface (TiC-layer) as well as a partial destruction of the diamond. On the diamond side these fracture characteristics except from the TiC-layer are visible, too (cf. Fig. 9d). Completely different shear surfaces were found for the specimens brazed at 980 °C, independent of the dwell duration (cf. Fig. 9e and f). The whole surface on the steel substrate as well as on the diamond is very smooth, indicating that the fracture directly occurs at the filler alloy-diamond interface. For the brazing parameters 880 °C and 930 °C for the dwell duration of 30 min the shear surfaces look similar to Fig. 9c and d. They exhibit the two fracture features partial destruction of the diamond and brittle fracture in the intermetallic interlayer at the steel-filler alloy interface. In addition it can be stated that the larger the area of the destroyed diamond the smaller the obtained shear strength.

Table 2

Shear strength values for the different brazing parameters.

Brazing parameters	Sample No.	Shear strength [MPa]	Diamond shattered
880 °C 10 min	1	208 ± 4	X
	2	420 ± 8	–
	3	335 ± 7	–
880 °C 30 min	1	196 ± 4	X
	2	318 ± 6	–
	3	150 ± 3	X
930 °C 10 min	1	188 ± 4	X
	2	220 ± 4	X
	3	189 ± 4	X
930 °C 30 min	1	116 ± 3	X
	2	137 ± 3	X
	3	166 ± 3	X
980 °C 10 min	1	75 ± 2	–
	2	78 ± 2	–
	3	61 ± 2	–
980 °C 30 min	1	42 ± 1	–
	2	60 ± 2	–
	3	–	–
	4	93 ± 2	–
	5	120 ± 3	–
	6	74 ± 2	–

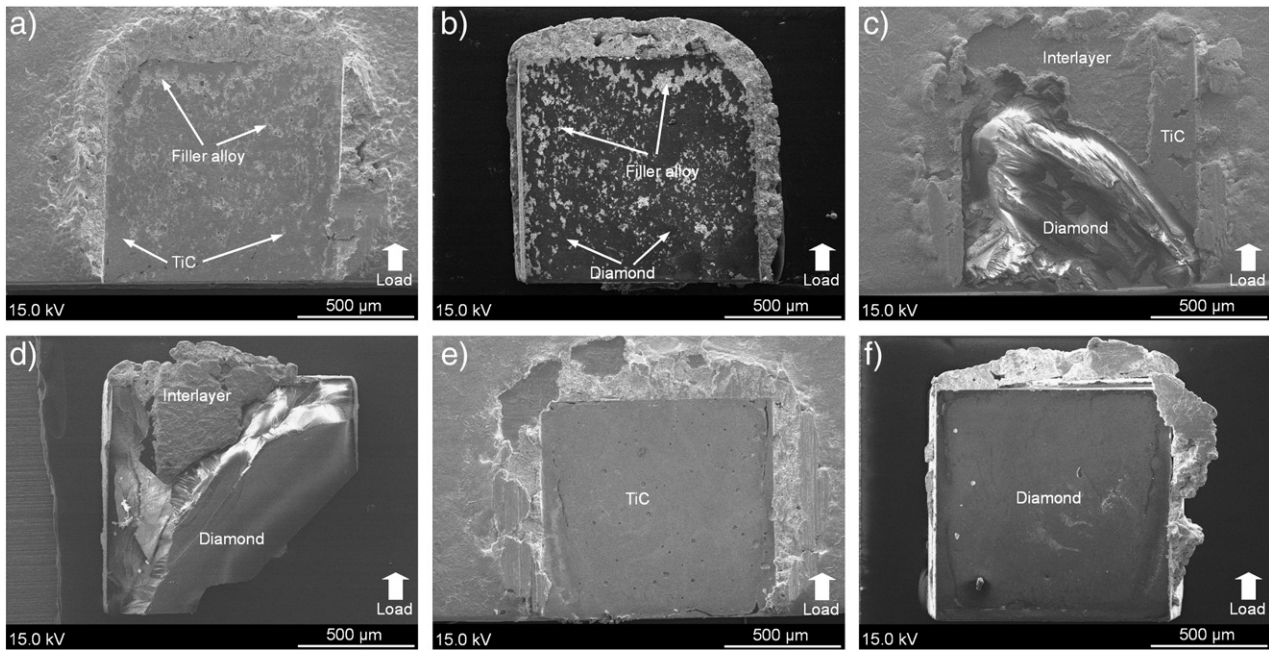


Fig. 9. Shear surfaces on the steel substrate (a, c and e) and those on the diamond side (b, d and f); 880 °C/10 min a), b); 930 °C/10 min c), d); 980 °C/10 min e), f). The arrows show the direction of the load introduction.

4. Discussion

The results above have shown that the brazing parameters strongly influence the brazing microstructure and hereby the diamond residual stresses as well as the shear strength. The discussion about the origins of this effect is divided into four parts namely the metallurgy of the filler alloy bond, the morphology of the filler alloy layer, the origin of residual stresses and their influence on the integrity of the filler alloy bond.

4.1. Filler alloy metallurgy

A prerequisite for the successful brazing of materials is the formation of interlayers at the interfaces of the partners to be joined. At the steel-filler alloy interface, the $(\text{Fe,Cr,Ni})_2\text{Ti}$ -type Laves-phase has formed while at the filler alloy-diamond interface a TiC layer can be assumed to exist, as has been reported in previous works [16,17]. However, the direct investigation of the TiC layer requires sophisticated, but time consuming Focused Ion Beam (FIB) preparation methods as well as transmission electron spectroscopy, which was out of the scope of the present work. Both interlayers grow with higher brazing temperature and holding time, which is due to accelerated diffusion processes and extended diffusion time. It was shown by other authors that the thickness of the TiC-layer can reach values of 600 nm for brazing parameters of 930 °C/100 min, when using the same filler alloy [16,17] or when annealing a titanium layer directly on a CVD diamond substrate at 500 °C for 120 min [61]. At a brazing temperature of 980 °C and 10 min holding time the thickness of the TiC-layer is almost twice as big as that of 930 °C, 10 min with a value of ~230 nm [16].

4.2. Filler alloy morphology

The brazing gap width decreases with higher brazing temperature which is due to a viscosity decrease of the molten filler alloy. A better spreading on the steel substrate is achieved and consequently the brazing gap width decreases. A decrease in the filler alloy thickness and an increase of the interlayer thickness result in an increase of the

percentage of brittle intermetallics with respect to the total filler alloy thickness.

4.3. Origin of residual stresses

Thermal residual stresses are the basis for the evolution of residual stresses in addition to volume changes of phase in the filler alloy layer due to phase transformation as well as the relaxation of stresses due to creep. The first form as a result of the different coefficients of thermal expansion (CTE) of the steel/filler alloy ($\alpha_{\text{steel}} = 16 \cdot 10^{-6} \text{ K}^{-1}$ [46]) and the diamond ($\alpha_{\text{diamond}} = 1.1 \cdot 10^{-6} \text{ K}^{-1}$ [62]).

The thermal residual stresses can be determined from the thermal strain ε_{th} , which can be calculated according to Eq. (3):

$$\varepsilon_{\text{th,diamond}} = \Delta\alpha \cdot \Delta T = (\alpha_{\text{diamond}} - \alpha_{\text{steel}}) \cdot \Delta T \quad (3)$$

where $\Delta\alpha = (\alpha_{\text{diamond}} - \alpha_{\text{steel}})$ is the mismatch in thermal expansion coefficients of diamond α_{diamond} and of the steel α_{steel} and ΔT is the difference between brazing temperature and room temperature. With $\Delta T = 860 \text{ K}$ the thermal strain in diamond is $\varepsilon_{\text{th,diamond}} = -0.013$. Using a Young's modulus of $E_{\text{diamond}} = 1050 \text{ GPa}$ given in Ref. [42] and considering only elastic deformation, the thermal residual stress in the diamond would be approximately -13.7 GPa , which is in a range of residual stresses measured in diamond films deposited via chemical vapour deposition CVD on various metallic substrates [62–65]. In these cases typically both the Raman–Stokes peak shifts strongly and the peak is split up, indicating high residual stresses in the range of at least several GPa.

Generally, the thermal expansion of the system will be solely determined by the thermal expansion of the steel substrate as is the mechanically strongest part. This is always true once the filler alloy is able to transmit stresses from the steel substrate to the diamond.

Let us start, however by considering high brazing temperatures at which the filler alloy is in a liquid state and consequently there is no or only a marginal mechanical coupling between diamond and steel substrate. At these temperatures a TiC layer is formed between the diamond and the filler alloy. Assuming epitaxial growth of this layer, a large lattice mismatch would be created at the diamond–TiC interface due to the misfit in the lattice parameter of the diamond

($a_{100} = 0.3566$ nm) and the TiC ($a_{100} = 0.4327$ nm) lattice. Due to this large difference of ~18% perfect coherency between the two lattices is very unlikely. A number of different defects at the interface, like stacking faults, micro-twins, misfit dislocations as well as grain boundaries in the polycrystalline TiC layer will form, leading to a stress relief [66–68]. Whether the TiC layer now introduces significant stresses in the diamond or vice-versa depends on the ratio of the respective products of Young's modulus and layer thickness. In all cases in this context the TiC layer is too thin compared to the diamond to introduce significant stresses in the diamond layer, however, its thickness will become important in the following considering the mechanical integrity of the bond.

Upon cooling the filler alloy starts solidifying and consequently introducing thermal stresses into the diamond. At this point the upper limit of residual stresses induced is determined by Eq. 3. In reality, the stresses are relieved during the cooling cycle of the brazing process by plastic deformation and creep of the filler alloy because of its low strength in comparison to diamond [62,69]. Creep is predominant at elevated temperatures. Compressive residual stresses are higher for brazing temperatures of 930 °C than for 880 °C. This is due to the fact that the brazing gap width scales inversely with temperature and plastic deformation is confined to a smaller volume at the higher brazing temperature which retards creep processes and leads to higher residual stresses.

Consequently, the residual stresses in diamond at room temperature are different from the theoretical values and are significantly lower in comparison to the strengths of the diamond (cf. Table 1).

4.4. Integrity of the bond

The results of the shear tests clearly show that the bond strength of diamonds on steel is strongly dependent of the microstructure as well as of the residual stresses in the diamond and in the filler alloy. It is obvious that the interlayers, i.e. the (Fe,Cr,Ni)₂Ti layer and the (Fe,Cr,Ni)₂Ti crystals at the steel/filler alloy interface and in particular the TiC layer at the filler alloy/diamond interface play an important role. A conclusion of the high measured hardnesses is that both interlayers rather behave in a brittle way. In contrast, the hardness of the matrix indicates a more ductile behaviour. The formation of additional intermetallic compounds in the (Cu,Sn)-matrix leads to a relatively high strength.

At the lowest brazing temperature of 880 °C, the (Fe,Cr,Ni)₂Ti-interlayer and the TiC-layer are rather thin in comparison with the overall brazing gap width ($d_{IL}/d_{gap} \approx 0.1$). It appears from the fracture surfaces (Fig. 9a and b) that fracture starts at the TiC/diamond interface and then propagates mainly along the interface but also in the filler alloy. With regard to the results of the Raman measurements, compressive residual stresses are present in the vicinity of the TiC/diamond interface. According to [16] the thin TiC layer has a cuboidal structure with rather smooth interfaces to the diamond and to the filler alloy, and relatively high stresses are necessary to initiate fracture.

At a brazing temperature of 980 °C, the TiC layer is significantly thicker. For this reason the probability of the presence of a critical flaw inside the TiC-layer is increased and therefore the fracture strength is decreased. In addition, tensile residual stresses are present at the TiC/diamond interface as shown in Fig. 7. Superposition with the external load leads to higher overall stresses in the TiC-layer. As a result cracks may nucleate more easily and propagate along the interface and in the TiC layer.

The shear test results for the specimens brazed at 930 °C are more difficult to interpret because the diamond fractured in almost all tests. The destruction of the diamond is most probably a result of a not exactly parallel alignment of the diamond and the shear plate. This can lead to a stress concentration in the diamond at the contact point to the shear plate, inducing cracks in the diamond. In these cases the fracture strength of diamond was tested rather than the bond strength.

However, the measured values can be taken as a lower boundary for the joint strength. Since this lower boundary for the joint strength is significantly higher than the shear strength for the specimens brazed at 980 °C, it can be assumed that the fracture characteristics are rather similar to those of the specimens brazed at 880 °C.

Obviously, there exists an upper threshold for the TiC-layer's thickness which should not be exceeded in order to avoid a strong decrease in shear strength. In the case of Ag–Cu based filler alloys with a lower Ti content and lower processing temperatures this threshold is not exceeded independently from the brazing parameters [41]. This shows that besides brazing parameters the composition of active brazing filler alloys and in particular the thermo-chemical properties of Ti are of significant importance for obtaining an optimal joint performance.

5. Summary and conclusions

In this work the influence of the brazing parameters, i.e. brazing temperature and dwell duration, on the properties of diamond–steel-joints was investigated. The specimen was a monocrystalline block-shaped diamond (MT L101005Q™) brazed with a Cu–Sn-based filler alloy (73.9 Cu–14.4 Sn–10.2 Ti–1.5 Zr, wt.%) onto a stainless steel substrate (X2CrNiMo 18–14–3). The major findings are:

- Formation of a (Cu,Sn)-matrix with different embedded intermetallic phases, like CuSn₃Ti₅, Cu₂SnTi, CuSnTi, NiTiSn and Ni₂TiSn as well as the formation of an intermetallic (Fe,Cr,Ni)₂Ti-interlayer at the steel-filler alloy interface.
- Strong dependence of the residual stresses on the brazing parameters, either the development of compressive (880 °C and 930 °C) or tensile residual stresses (980 °C). The highest compressive residual stress appears with about –350 MPa at 930 °C for 10 min holding time.
- Decrease in shear strength with higher brazing temperature and longer holding time. Decrease from (321 ± 107) MPa for samples brazed at 880 °C for 10 min to (71 ± 9) MPa for samples brazed at 980 °C for 10 min. At the lower brazing temperature the fracture path partly proceeds through the ductile filler alloy, whereas at the higher brazing temperature the TiC-layer is the weakest element. In this case the TiC-layer becomes too thick, assuming that the upper threshold for the TiC-layer thickness is exceeded.

We found, that in contrast to the experiments done with an Ag–Cu based active filler alloy [41], the residual stresses as well as the shear strength strongly depend on the brazing parameters. Therefore, if this filler alloy is used, the brazing parameters should be carefully chosen, based on the most important required characteristic.

Acknowledgements

The authors would like to thank the Swiss National Science Foundation for the financial support under the number 200021-117847. S.B. is grateful to Dr. H.-R. Elsener (Laboratory for Joining and Interface Technology, Empa, Dübendorf) for his support in brazing and Dr. T. Wermelinger (Laboratory for Nanometallurgy, ETH, Zurich) for fruitful discussions about Raman-spectroscopy.

References

- [1] Hintermann HE, Chattopadhyay AK. New generation superabrasive tool with monolayer configuration. *Diamond Relat Mater* 1992;1:1131–43.
- [2] Sung CM. Brazed diamond grid: a revolutionary design for diamond saws. *Diamond Relat Mater* 1999;8:1540–3.
- [3] Sung JC, Sung M. The brazing of diamond. *Int J Refract Met Hard Mater* 2009;27:382–93.
- [4] Huang SF, Tsai HL, Lin ST. Laser brazing of diamond grits using a Cu–15Ti–10Sn brazing alloy. *Mater Trans* 2002;43:2604–8.

- [5] Chattopadhyay AK, Chollet L, Hintermann HE. Experimental investigation on induction brazing of diamond with Ni–Cr hardfacing alloy under Argon atmosphere. *J Mater Sci* 1991;26:5093–100.
- [6] Chattopadhyay AK, Chollet L, Hintermann HE. Induction brazing of diamond with Ni–Cr hardfacing alloy under Argon atmosphere. *Surf Coat Technol* 1991;45:293–8.
- [7] Lee C, Ham J, Song M. The interfacial reaction between diamond grit and Ni-based brazing filler metal. *Mater Trans* 2007;48:889–91.
- [8] Ma BJ, Fu YC, Ding WF, Gao W, Xu HJ. Research on interfacial microstructure of Ti-coated diamond brazed and uncoated diamond brazed by high-frequency induction. *Adv Grind Abr Tech* 2008;359–360:53–7.
- [9] Chen JY, Huang H, Xu XP. An experimental study on the grinding of alumina with a monolayer brazed diamond wheel. *Int J Adv Manuf Technol* 2009;41:16–23.
- [10] Fernandes AJS, Fonseca MJ, Costa FM, Silva RF, Nazare MH. Ultramicrohardness cross-profiling of CVD diamond–steel brazed junctions. *Diamond Relat Mater* 1999;8:855–8.
- [11] Kohzaki M, Higuchi K, Noda S, Uchida K. Large-area diamond deposition and brazing of the diamond films on steel substrates for tribological applications. *Diamond Relat Mater* 1993;2:612–6.
- [12] Shiue RK, Buljan ST, Eagar TW. Abrasion resistant active braze alloys for metal single layer technology. *Sci Technol Weld Joining* 1997;2:71–8.
- [13] Tillmann W, Osmanda AM. Production of diamond tools by brazing. *Front Process Eng Adv Mater* 2005;502:425–30.
- [14] Trenker A, Seidemann H. High-vacuum brazing of diamond tools. *Ind Diamond Rev* 2002;62:49–51.
- [15] Moret E, Eustathopoulos N. Ceramic-to-metal direct brazing. *J Phys IV* 1993;3:1043–52.
- [16] Klotz UE, Liu CL, Khalid FA, Elsener HR. Influence of brazing parameters and alloy composition on interface morphology of brazed diamond. *Mater Sci Eng, A* 2008;495:265–70.
- [17] Liu CL. Characterisation and Modelling of Interface Reactions between Diamond and Active Brazing Alloys. PhD-Thesis, Eidgenössische Technische Hochschule Zürich ETHZ, Switzerland, 2007.
- [18] Yulyugin SV, Kolesnichenko GA, Yulyugin VK, Evdokimov VA, Naidich YV. Adhesion and wetting in diamond – and carbide – melt systems and the liquid phase sintering of composites on their base. In: Kumar A, Chung YW, Moore JJ, Smugersky JE, editors. *Surface engineering: science and technology I*. Warrendale, PA: The Minerals, Metals & Materials Society; 1999. p. 453–61.
- [19] Kizikov ED, Kebko VP. Microadditions to alloys of the system Cu–Sn–Ti. *Met Sci Heat Treat* 1987;29:68–71.
- [20] Saarivirta MJ. Development of copper base high strength – medium conductivity alloys – Cu–Sn–Ti and Cu–Sn–Ti–Cr. *Trans Metall Soc AIME* 1961;221:596–606.
- [21] Evens D, Nicholas M, Scott PM. Wetting and bonding of diamonds by copper–titanium alloys. *Ind Diamond Rev* 1977;306–9.
- [22] Hamar-Thibault S, Allibert CH. New phases in the ternary Cu–Ti–Sn system. *J Alloys Compd* 2001;317:363–6.
- [23] Heine W, Zwicker U. Phasen des B2-Strukturtyps (CsCl-Typ) in ternären Systemen mit Kupfer und Nickel. *Naturwiss* 1962;49:391.
- [24] Hsieh YC, Lin ST. Microstructural development of Cu–Sn–Ti alloys on graphite. *J Alloys Compd* 2008;466:126–32.
- [25] Huang SF, Tsai HL, Lin ST. Crystal structure and X-ray diffraction pattern of CuSnTi₃ intermetallic phase. *Intermet* 2005;13:87–92.
- [26] Schuster JC, Naka M, Shibayanagi T. Crystal structure of Cu₃SnTi₅ and related phases. *J Alloys Compd* 2000;305:L1–3.
- [27] Weitzer F, Perring L, Shibayanagi T, Naka M, Schuster JC. Determination of the crystal structure of Cu₃SnTi by full profile Rietveld analysis. *Powder Diffr* 2000;15:91–3.
- [28] Liu CL, Klotz UE, Löffler JF. Cu–Sn–Ti (Copper–Tin–Titanium). In: Effenberg G, Ilyenko S, editors. *Non-ferrous metal ternary systems selected soldering and brazing systems: phase diagrams, crystallographic and thermodynamic data: SpringerMaterials – the Landolt-Börnstein database*; 2007. p. 409–21.
- [29] Elsener HR, Klotz UE, Khalid FA, Piazza D, Kiser M. The role of binder content on microstructure and properties of a Cu-base active brazing filler metal for diamond and cBN. *Adv Eng Mater* 2005;7:375–80.
- [30] Bonera E, Fanciulli M, Batchelder DN. Combining high resolution and tensorial analysis in Raman stress measurements of silicon. *J Appl Phys* 2003;94:2729–40.
- [31] De Wolf I. Micro-Raman spectroscopy to study local mechanical stress in silicon integrated circuits. *Semicond Sci Technol* 1996;11:139–54.
- [32] De Wolf I. Raman spectroscopy: about chips and stress. *Spectrosc Eur* 2003;15:6–13.
- [33] De Wolf I, Maes HE, Jones SK. Stress measurements in silicon devices through Raman spectroscopy: bridging the gap between theory and experiment. *J Appl Phys* 1996;79:7148–56.
- [34] Wermelinger T, Borgia C, Solenthaler C, Spolenak R. 3-D Raman spectroscopy measurements of the symmetry of residual stress fields in plastically deformed sapphire crystals. *Acta Mater* 2007;55:4657–65.
- [35] Dos Santos SI, Balzaretto NM, Da Jornada JAH. Adhesion between CVD diamond and WC-Co induced by high-pressure and high-temperature. *Diamond Relat Mater* 2006;15:1457–61.
- [36] Klocke F, Merbecks T. Characterization of vitrified cBN grinding wheels. 4th International Machining and Grinding Conference. SME Conf Proc, Troy MI; 2001.
- [37] Naidich YV, Umanskii VP, Lavrinenko IA. Strength of the diamond–metal interface and brazing of diamonds. Cambridge: Cambridge International Science Publishing Ltd; 2007.
- [38] Yamazaki T, Suzumura A. Reaction products at brazed interface between Ag–Cu–V filler metal and diamond (111). *J Mater Sci* 2006;41:6409–16.
- [39] Yamazaki T, Suzumura A. Relationship between X-ray diffraction and unidirectional solidification at interface between diamond and brazing filler metal. *J Mater Sci* 2000;35:6155–60.
- [40] Siegmans S, Dvorak M, Gruetzner H, Nassenstein K, Walter A. Shear testing for characterizing the adhesive and cohesive coating strength without the need of adhesives. *Proc Int Therm Spray Conf* 2005; 2005. p. 823–9.
- [41] Buhl S, Leinenbach C, Spolenak R, Wegener K. Influence of the brazing parameters on microstructure, residual stresses and shear strength of diamond–metal joints. *J Mater Sci* 2010;45:4358–68.
- [42] Field JE. The properties of diamond. London: Academic Press; 1979.
- [43] Field JE. Strength, fracture and erosion properties of diamond. In: Field JE, editor. *The properties of natural and synthetic diamond*. London: Academic Press; 1992. p. 473–513.
- [44] Field JE. Cleavage, fracture and tensile strength of diamond. In: Davies G, editor. *Properties and growth of diamond*. London: INSPEC; 1994. p. 36–51.
- [45] Kizikov ED, Lavrinenko IA. Investigations of Cu–Sn–Ti alloys used for bonding diamond abrasive tools. *Met Sci Heat Treat* 1975;17:61–5.
- [46] Wegst C, Wegst M. Nachschlagewerk Stahlschüssel. Verlag Stahlschüssel Wegst GmbH, Marbach; 2007.
- [47] Ikawa N, Shimada S, Ono T. Microstrength of diamond. *Technol Rep Osaka Univ* 1976;26:245–54.
- [48] Anastassakis E, Pinczuk A, Burstein E, Pollak FH, Cardona M. Effect of static uniaxial stress on Raman spectrum of silicon. *Solid State Commun* 1970;8:133–8.
- [49] Cousins CSG. Elasticity of carbon allotropes. I. Optimization, and subsequent modification, of an anharmonic Keating model for cubic diamond. *Phys Rev B: Condens Matter* 2003;67:241071–2410713.
- [50] Englert T, Abstreiter G, Pontcharra J. Determination of existing stress in silicon films on sapphire substrate using Raman-spectroscopy. *Solid-State Electron* 1980;23:31–3.
- [51] Ganesan S, Maradudin AA, Oitmaa J. A lattice theory of morphic effects in crystals of diamond structure. *Ann Phys* 1970;56:556–94.
- [52] Klocke P. Handbook of infrared optical materials. New York: Marcel Dekker, Inc.; 1991.
- [53] Duarte LI, Klotz UE, Leinenbach C, Palm M, Stein F, Löffler JF. Experimental study of the Fe–Ni–Ti system. *Intermet* 2010;18:374–84.
- [54] Compton DN, Leitch AWR, Neethling JH, Kozyrkov VV. A microstructural analysis of thin film TiNiSn. *Proc 15th Int Conf Thermoelectr*; 1996. p. 491–3.
- [55] Dvorakova H. Study of properties of metal solder. *Kovove Mater* 1985;5:629–38.
- [56] Khalid FA, Klotz UE, Elsener HR, Zigerlig B, Gasser P. On the interfacial nanostructure of brazed diamond grits. *Scripta Mater* 2004;50:1139–43.
- [57] Marchuk ND, Skolozdra RV, Stadnyk YV. Thermoelectric properties of new intermetallic compounds MMSn. *Proc 14th Int Conf Thermoelectr*; 1995. p. 217–21.
- [58] Tan ZS, Jesser WA. Microstructure analysis of thermoelectric TiNiSn alloy. *Proc 14th Int Conf Thermoelectr*; 1995. p. 249–53.
- [59] Rieger W, Nowotny H, Benesovsky F. Verbindungen mit aufgefüllten Mn₅Si₃-Typ. *Monatsh Chem* 1965;96:98–103.
- [60] Rieger W, Nowotny H, Benesovsky F. Phasen mit oktaedrischen Bauelementen des Übergangsmetalls. *Monatsh Chem* 1965;96:232–41.
- [61] Zhu Y, Zheng B, Yao W, Cao L. The interface diffusion and chemical reaction between a Ti layer and a diamond substrate. *Diamond Relat Mater* 1999;8:1073–8.
- [62] Groegler T, Zeiler E, Hoerner A, Rosiwal SM, Singer RF. Microwave-plasma-CVD of diamond coatings onto titanium and titanium alloys. *Surf Coat Technol* 1998;98:1079–91.
- [63] Chen KH, Lai YL, Lin JC, Song KJ, Chen LC, Huang CY. Micro-Raman for diamond film stress analysis. *Diamond Relat Mater* 1995;4:460–3.
- [64] Fan QH, Gracio J, Pereira E, Teixeira V, Tavares CJ. Determination of biaxial modulus of chemical vapor-deposited diamond films. *Thin Solid Films* 2001;398:265–9.
- [65] Ralchenko VG, Obratzsova ED, Korotushenko KG, Smolin AA, Pimenov SM, Pereverzev VG. Stress in thin diamond films on various materials measured by microRaman spectroscopy. Mechanical behavior of diamond and other forms of carbon. *Mater Res Soc Symp ProcPittsburgh, PA: Materials Research Society*; 1995. p. 153–8.
- [66] Huang SF, Tsai HL, Lin ST. Effects of brazing route and brazing alloy on the interfacial structure between diamond and bonding matrix. *Mater Chem Phys* 2004;84:251–8.
- [67] Li WC, Liang C, Lin ST. Epitaxial interface of nanocrystalline alloy and TiC formed between Cu–10Sn–15Ti diamond. *Diamond Relat Mater* 2002;11:1366–73.
- [68] Li WC, Liang C, Lin ST. Interfacial segregation of Ti in the brazing of diamond grits onto a steel substrate using a Cu–Sn–Ti brazing alloy. *Metall Mater Trans A* 2002;33:2163–72.
- [69] Scardi P, Leoni M, Cappuccio G, Sessa V, Terranova ML. Residual stress in polycrystalline diamond Ti–6Al–4 V systems. *Diamond Relat Mater* 1997;6:807–11.